Available online at www.sciencedirect.com
ScienceDirect
Earth and Planetary Science Letters 260 (2007) 166–178
EPSL
www.elsevier.com/locate/epsl

Raman spectroscopy of perovskite and post-perovskite phases of $MgGeO_3$ to 123 GPa

Sang-Heon Shim [a,*], Atsushi Kubo [b,1], Thomas S. Duffy [b]

[a] Department of Earth, Atmospheric, and Planetary Sciences, Massachusetts Institute of Technology, Cambridge, Massachusetts, USA
[b] Department of Geosciences, Princeton University, Princeton, New Jersey, USA

Received 3 April 2007; received in revised form 14 May 2007; accepted 19 May 2007
Available online 26 May 2007
Editor: G.D. Price

Abstract

Raman spectra of the perovskite (Pv) and post-perovskite (PPv) phases of $MgGeO_3$ were measured in the laser-heated diamond cell up to 123 GPa. Between 14 and 51 GPa we observed a total of seven Pv modes, the frequencies and relative intensities of which are similar to $MgSiO_3$–Pv with systematically lower frequencies. We also observe a total of ten PPv modes which are much more intense than Pv modes, indicating strong polarizability of the bonds in PPv. The observed Raman mode frequency range of PPv extends to much higher frequencies than Pv, which can be related to the edge sharing of the GeO_6 octahedra in PPv which would make Ge–O bonds stronger. The spectroscopic Grüneisen parameters of Pv and PPv are constrained to be 1.56 ± 0.10 and 1.15 ± 0.06, respectively, at the PPv transition. We also estimated that the thermal expansion parameter decreases by $25\pm10\%$ across the PPv transition. If a similar change occurs in $MgSiO_3$, the low thermal expansivity would dynamically stabilize the PPv layer at the lowermost mantle. Using our Raman measurements and a Kieffer-type model, the Clapeyron slope of the PPv transition is constrained to be $+20\pm10$ MPa/K. The strong positive slope is consistent with the prediction for $MgSiO_3$ and is related to a positive shift of phonon density of states at high-frequency region resulting from the formation of the edge sharing among the GeO_6 (or SiO_6) octahedra in PPv.

Keywords: perovskite; post-perovskite; Raman spectroscopy; Grüneisen parameter; thermal expansivity; Clapeyron slope

1. Introduction

The recent discovery of a phase transition in $MgSiO_3$–perovskite (Pv) at conditions of the lowermost mantle, the post-perovskite (PPv) transition (Murakami et al., 2004; Oganov and Ono, 2004; Shim et al., 2004), has impacted our understanding of seismic observations and dynamics of the region [e.g., (Lay et al., 2005, 2006)]. A strong positive Clapeyron slope has been proposed for the PPv transition from theoretical calculations, +7∼10 MPa/K (Oganov and Ono, 2004; Iitaka et al., 2004; Tsuchiya et al., 2004; Sternik and Parlinski, 2006), which is consistent with seismic observations of the D'' discontinuity (Sidorin et al., 1999). This strong positive Clapeyron slope may affect dynamics of the core–mantle boundary region (Nakagawa and Tackley, 2004; Matyska and Yuen, 2005).

Changes in thermodynamic properties across the PPv transition have not been well constrained by experiments. It is challenging to carry out X-ray measurements of

* Corresponding author.
E-mail address: sangshim@mit.edu (S.-H. Shim).
[1] Now at CARS, University of Chicago, Illinois, USA.

0012-821X/$ - see front matter © 2007 Elsevier B.V. All rights reserved.
doi:10.1016/j.epsl.2007.05.027

pressure (P)–volume (V)–temperature (T) relations for the determination of accurate thermal equation of state (EOS) at the stable P–T conditions for $MgSiO_3$–PPv, 125–140 GPa and 2000–3000 K, in the laser-heated diamond-anvil cell (LHDAC) due to large thermal gradients and uncertainties in temperature measurements (Boehler, 2000; Kiefer and Duffy, 2005). In a recent X-ray study of $MgSiO_3$–PPv (Guignot et al., 2007), additional constraints from theoretical studies were necessary to obtain some thermal parameters due to a limited P range (110–145 GPa) of the measurement. The fact that the expected radial temperature gradients at the D'' layer are comparable to that of the Clapeyron slope of the PPv transition enables constraints to be placed on heat flux out of the outer core combined with seismic observations of the double crossings (Hernlund et al., 2005; Shim, 2005; Lay et al., 2006; van der Hilst et al., 2007). However, unambiguous determination of the slope is very challenging using in situ X-ray diffraction (XRD) because of sluggishness of the PPv transition, preferred orientation, and thermal gradients in LHDAC (Hirose et al., 2006). Furthermore, inconsistency among the internal X-ray pressure scales (Shim et al., 2002) can also cause large uncertainties in measured Clapeyron slope.

Vibrational spectroscopy, such as infrared (IR) and Raman spectroscopy, can provide important constraints on crystal structures and thermodynamic properties of materials. These measurements have been successfully conducted for many mantle minerals in the diamond-anvil cell (DAC) [e.g., (Williams et al., 1987; Lu and Hofmeister, 1994; Chopelas, 1996, 1999)]. In particular, the Grüneisen parameter can be obtained by monitoring P-induced shifts of phonon modes. By making assumptions about the phonon density of states (PDOS), such as Kieffer's model, data from vibrational spectroscopy can also constrain geophysically important parameters, including heat capacity, thermal expansivity, entropy, and Clapeyron slope (Kieffer, 1979a,b, 1982).

Magnesium germanates are known to be good analogs for magnesium silicates (Ross and Navrotsky, 1988; Akaogi et al., 2005; Kubo et al., 2006; Runge et al., 2006). They undergo a similar sequence of phase transitions but at lower P. $MgGeO_3$–Pv undergoes a phase transition to PPv at 60–70 GPa (Hirose et al., 2005) which is much lower than that in $MgSiO_3$, 125 GPa. Raman measurements on $MgSiO_3$–PPv are challenging due to technical issues at its stable P conditions ($\geq$125 GPa), including strong fluorescence from diamond anvils (Xu et al., 1986) and extremely weak signal from spectroscopic pressure scales, such as ruby (Eggert et al., 1988). Therefore, $MgGeO_3$ provides opportunities to measure high-quality Raman spectra of PPv at lower P.

2. Experimental techniques

Pure $MgGeO_3$ orthopyroxene (OPx) sample was synthesized by heating a mixture of MgO and GeO_2 in air at 1300 K for 40 h. The same sample has been used in recent high P measurements (Kubo et al., 2006; Runge et al., 2006; Merkel et al., 2006). A platinum foil was sandwiched between two $MgGeO_3$ foils and the assembly was loaded in a Re gasket hole in a DAC with an Ar pressure medium. In order to prevent direct contact between the sample and the diamonds, spacer grains of $MgGeO_3$ were placed at the top and the bottom of the foil. Ruby grains were placed near the edge of the hole to serve as a pressure calibrant (Mao et al., 1986). Diamond anvils with 300-μm flat and 150-μm beveled culets were used for measurements up to 55 GPa and 123 GPa, respectively.

Raman modes were excited by a 514.5-nm beam of an Ar/Kr mixed ion laser at MIT. The laser power at the sample is controlled to less than 10 mW. The Raman spectra were collected using a CCD detector attached to a 0.5-m single spectrometer with collection times of 10–15 min. The size of the focused beam at the sample was less than 5 μm in diameter. The spectrometer was calibrated from Ne spectral lines.

In order to synthesize stable high-P phases and to reduce deviatoric stresses, the samples were heated using a Nd:YLF laser (TEM_{00}) to 2000 K for 10 min for synthesis and to 1500 K for 2 min for stress annealing before each Raman measurement. In order to reduce heterogeneity in stress conditions, we scanned the sample across the laser beam. The size of the heating spot was about 20 μm in diameter. Background spectra were collected from a location in the gasket hole containing only Ar.

3. Results

During compression at room T, Raman modes of $MgGeO_3$–OPx disappeared at 24 GPa (Fig. 1a–b) and some broad features were observed at higher-frequency region (700–1000 cm^{-1}). In X-ray measurements at similar pressures, the diffraction lines of OPx were no longer observed and some weak and broad new peaks appeared (A. Kubo, personal communication). These observations imply that the phase is crystalline but possibly highly disordered.

After laser heating at 33 GPa, we observed six Raman modes (Fig. 1). The highest frequency peak shows asymmetry and splits into two peaks at higher P (ν_6 and ν_7 in Fig. 1c–e). Thus, we identify a total of seven Raman modes for $MgGeO_3$–Pv at high P.

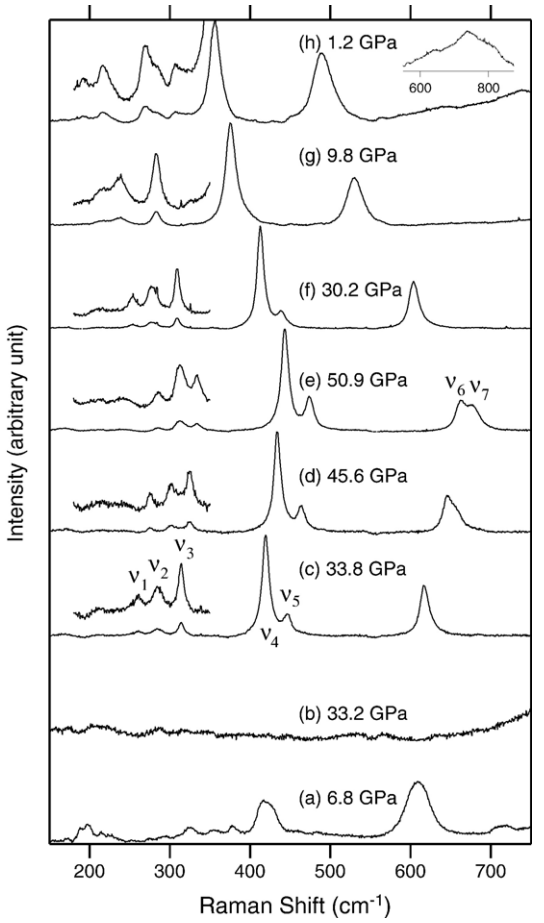

Fig. 1. Raman spectra of $MgGeO_3$–Pv measured during compression (c–e) and decompression (f–h). (a) Raman spectrum of the starting material, OPx. (b) Raman spectrum of the sample before the first laser heating at 33.2 GPa. The insets for low-frequency regions show weak modes. The inset at high frequency in (h) shows a broad spectral feature developed during decompression. The modes were tentatively assigned (ν_1–ν_7) in the order of their frequencies. Backgrounds were subtracted from the spectra.

The observed peaks become sharper after laser annealing, indicating that deviatoric stresses are effectively reduced.

From group theory for *Pbnm* perovskite, 24 out of 60 total phonon modes are Raman active. In an earlier measurement on $MgSiO_3$–Pv by Williams et al. (1987), only four modes were observed at ambient conditions. Chopelas (1996) documented a total of nine and six Raman modes below and above 40 GPa, respectively. The weak intensity and limited number of observed Raman modes has been attributed to the relatively small distortion in $MgSiO_3$–Pv from an ideal cubic perovskite structure (Williams et al., 1987). The *b*/*a* and *c*/*a* ratios of $MgGeO_3$–Pv are only 1.0 and 1.3% higher than those of $MgSiO_3$–Pv at 0–65 GPa (Runge et al., 2006), indicating the crystal structure of $MgGeO_3$–Pv is very similar to that of $MgSiO_3$–Pv.

In order to prevent a reverse transformation to low-*P* phases, we did not laser anneal the samples during decompression, resulting in broader peaks (Fig. 1f–h). Nevertheless, the mode frequencies agree well with compression data within the Pv stability field (Fig. 2). However, below 14 GPa, the mode frequencies decrease with higher rates, due perhaps to the metastability of Pv. A spectrum measured at 1.2 GPa (Fig. 1h) shows some new features, such as a broad feature above 600 cm^{-1}, indicating a partial transformation to a low-*P* phase.

A separate sample was compressed without heating to 82.7 GPa which is well above the reported PPv boundary in $MgGeO_3$, 60–70 GPa (Hirose et al., 2005) (Fig. 3). Broad modes of the unknown $MgGeO_3$ phase were also observed to this pressure. After laser heating, a total of 10 peaks were observed. The PPv modes are extremely intense: the maximum number of counts for PPv at 123 GPa is two orders of magnitude higher than for Pv at 33 GPa for a given collection time. This indicates strong polarizability of the bonds in PPv. A spectral feature at 750 cm^{-1} (N_5–N_7) shows severe asymmetry and a structure at the lower-frequency shoulder. As shown in the inset of Fig. 3e, three symmetric peaks are necessary in order to fit the feature. A weak

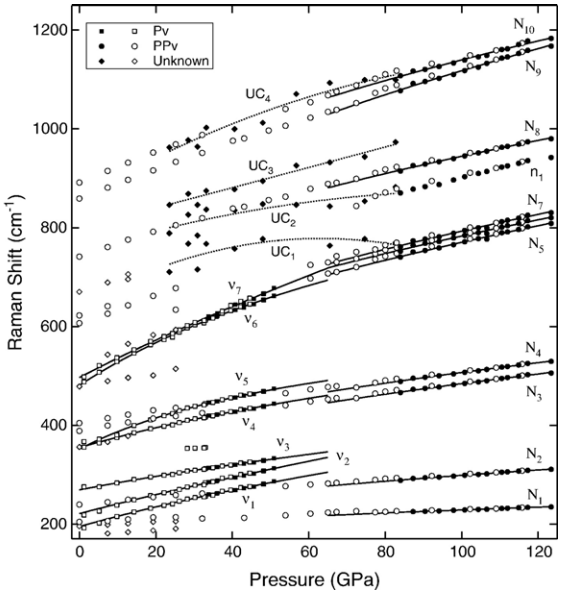

Fig. 2. Pressure-induced shifts of the Raman modes of Pv (square), PPv (circle), and unknown phase (diamond) in $MgGeO_3$. Solid and open symbols represent data measured during compression and decompression, respectively. Fitting of the data is shown by curves. The size of error bar for mode frequency is smaller than that of the symbols. Uncertainty in pressure is 3%. The frequencies of the modes observed only during cold compression are also shown (UC_1–UC_4).

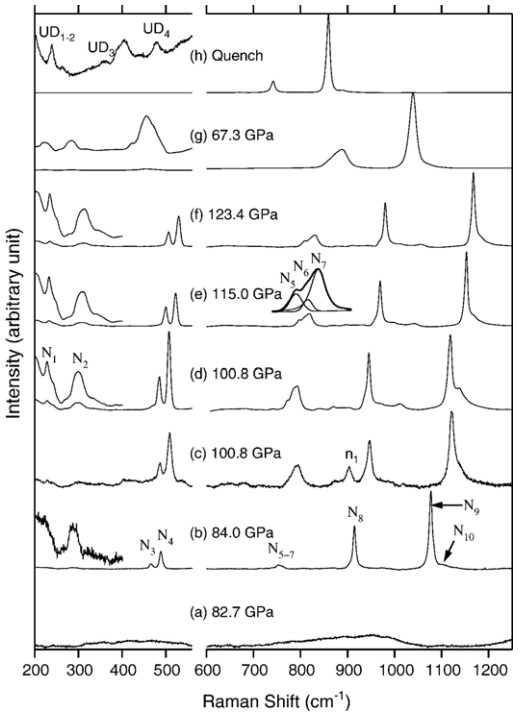

Fig. 3. Raman spectra of $MgGeO_3$–PPv measured during compression (b–f) and decompression (g–h). (a) Raman spectrum of the sample before the first laser heating. The insets show expanded view of weak modes (b,d–h) and peak asymmetry (e). (c) and (d) are measured at different locations in the same sample at the same load. Modes were tentatively assigned (N_1–N_{10}) in the order of their frequencies. In order to cover a wide spectral range, we measured low- and high-frequency regions (below and above 600 cm^{-1}), separately. Backgrounds were subtracted from the spectra.

feature exists at the higher-frequency side of the most intense peak (N_{10}). The peak becomes clear at 101 GPa (Fig. 3d).

Only a few Raman measurements have been reported on PPv-structured materials. Four Raman modes were resolved between 200 and 800 cm^{-1} in $CaIrO_3$ at ambient conditions (Hirose and Fujita, 2005). Due to the limited spectral coverage for $CaIrO_3$, relating the Raman spectrum of $CaIrO_3$ to $MgGeO_3$–PPv is not straightforward. Mn_2O_3 transforms to a PPv-structured phase at 30–40 GPa and 300 K (Santillán et al., 2006). Our Raman spectra of Mn_2O_3–PPv show nine strong modes between 100 and 900 cm^{-1} at 29 GPa. There are striking similarities between the $MgGeO_3$ and Mn_2O_3 spectra (Fig. 4): N_1 and N_2 appear similar to modes at 170 and 235 cm^{-1} in Mn_2O_3–PPv, respectively. N_{3-4} and N_{5-7} can be related to the multiplets at 370 and 560 cm^{-1}, respectively. Two high-frequency modes, N_8 and N_9, can be related to modes at 650 and 790 cm^{-1}, respectively. Not only relative positions but also relative intensities among peaks are noticeably similar, even though $MgGeO_3$ is chemically very different from Mn_2O_3. Between 500 and 600 cm^{-1}, Mn_2O_3–PPv shows a broad feature that appears to consist of at least two peaks. The asymmetry of the lower-frequency structure suggests that it consists of 3 peaks similar to N_{5-7} in $MgGeO_3$–PPv.

In $MgGeO_3$, another peak is observed at 900 cm^{-1} in one area of the sample throughout our measurements (n_1 in Fig. 3c). This peak could be interpreted as a highly orientation sensitive mode, provided that $MgGeO_3$–PPv can develop significant degree of lattice preferred orientation which has been reported in not only $MgGeO_3$–PPv (Merkel et al., 2006) but also other PPv structured materials (Santillán et al., 2006; Miyajima et al., 2006). It is also possible that this peak is from an impurity which may be present in the starting material or dissociation product of $MgGeO_3$, such as GeO_2. However, the mode does not match with expected behaviors of rutile or $CaCl_2$-type GeO_2 (Fig. 5). Furthermore, previous X-ray studies on $MgGeO_3$–Pv and –PPv did not observe any evidence of dissociation (Kubo et al., 2006; Runge et al., 2006). GeO_2 is known to transform to an α-PbO_2-type phase at 40 GPa. Because the Raman spectrum of the α-PbO_2-type phase is not known, we do not include this peak in our analysis.

A mode at 300 cm^{-1}, N_2 , is broader than the other observed peaks. The peak remains symmetric throughout our measurements. Therefore, we treat this as a

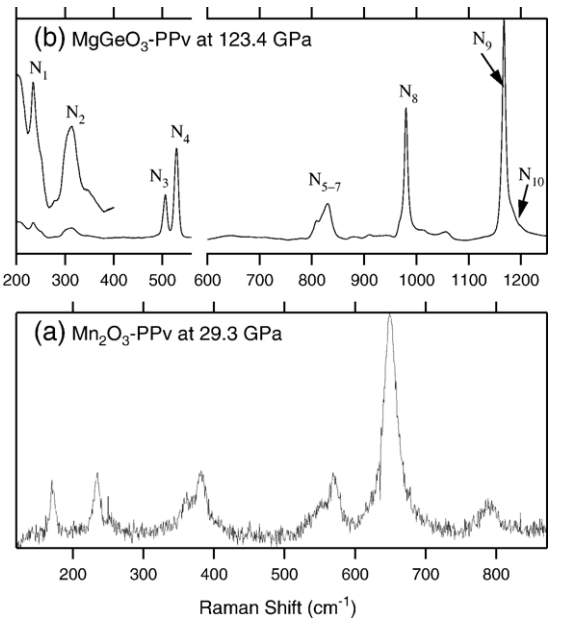

Fig. 4. Raman spectra of (a) Mn_2O_3– and (b) $MgGeO_3$–PPv.

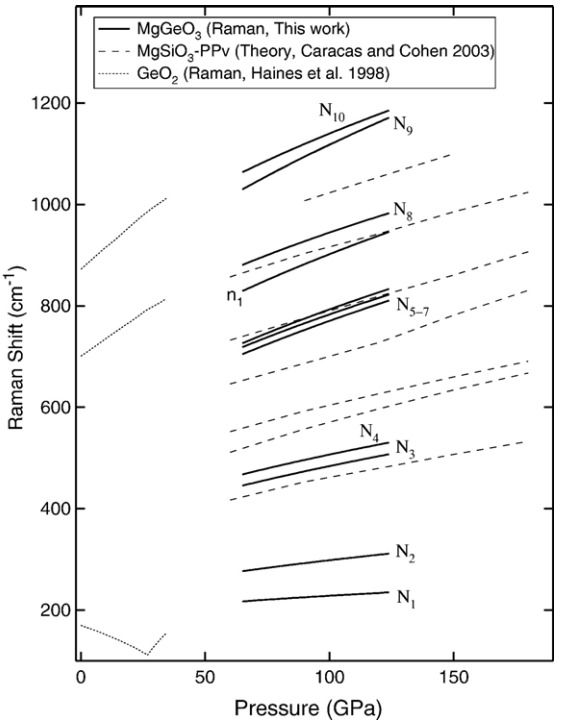

Fig. 5. Pressure-induced shifts of the Raman modes of $MgGeO_3$–PPv (solid lines) compared with rutile-type GeO_2 (dotted lines) (Haines et al., 1998) and $MgSiO_3$–PPv (dashed lines) (Caracas and Cohen, 2006). The mode frequencies of $MgSiO_3$–PPv were obtained by fitting the peaks in the calculated spectra published in Caracas and Cohen (2006). Only 7 modes have resolvable intensities in these spectra.

singlet. However, the width could indicate that the peak consists of two adjacent modes with similar intensities. It is notable that a related feature in PPv-structured Mn_2O_3 at 220–260 cm^{-1} consists of two peaks, i.e., one stronger and the other weaker (Fig. 4). If the peak is a doublet and n_1 is also from $MgGeO_3$–PPv, then the number of observed PPv modes increases to twelve. For the primitive cell of PPv (space group *Cmcm*), a total of 12 among 30 phonon modes are Raman active, so most or all Raman active modes have been identified.

With decompression, widths of the peaks increase. Moreover, the frequencies are systematically higher than those under compression and decrease nonlinearly (Fig. 2). This may be related to lack of annealing during decompression. Below 67 GPa, we observe a significant decrease in intensities of the low-frequency modes, which may be due to the metastability of PPv. Below 25 GPa, five unknown modes appear and persist to ambient P (open diamonds in Fig. 2). This indicates a phase transition of PPv upon decompression to an unknown crystalline phase, which persists to ambient conditions.

4. Discussion

4.1. Raman spectra of $MgGeO_3$–Pv and–PPv

Because polarized Raman measurements for appropriate single crystals do not exist, mode assignments remain uncertain for $MgSiO_3$– and $MgGeO_3$–Pv. Using systematics among perovskite-structured materials, a Raman mode of $MgSiO_3$–Pv at 499 cm^{-1} was assigned to a breathing vibration of the SiO_6 octahedra (Williams et al., 1987). Also modes at 378 cm^{-1} and 251–280 cm^{-1} are related to a symmetric stretching vibration of the SiO_6 octahedra, and octahedral rotation and deformation coupled with displacement of cations in the dodecahedral sites, respectively. $MgGeO_3$–Pv has the same structure as $MgSiO_3$–Pv with similar degree of distortions. Furthermore, observed relative intensities among modes are very similar between $MgGeO_3$– and $MgSiO_3$–Pv. Therefore, the contrast between Ge and Si could also help make mode assignments.

The extrapolated frequencies of $MgGeO_3$–Pv modes are lower by $\Delta\nu = 13–55$ cm^{-1} compared with corresponding modes of $MgSiO_3$–Pv at ambient P (Fig 6). Lower-frequency modes, ν_1–ν_5, appear to be more sensitive to the cation change ($\Delta\nu = 27–55$ cm^{-1}

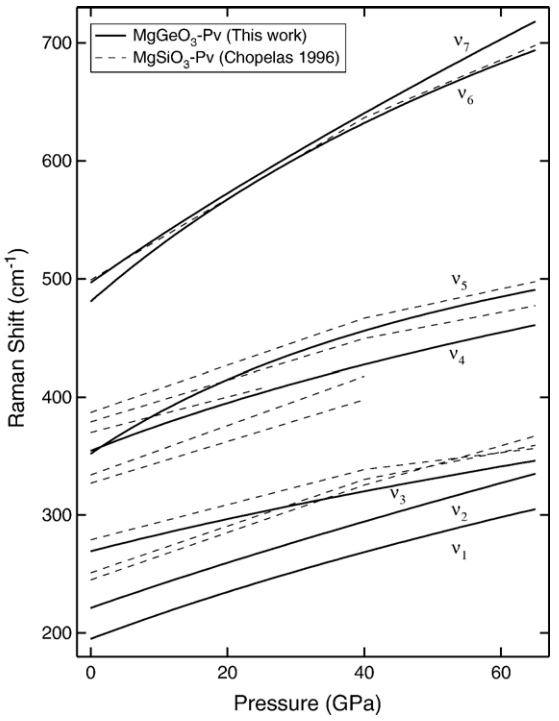

Fig. 6. Pressure-induced shifts of the Raman modes of $MgGeO_3$– (solid lines) and $MgSiO_3$– (dashed lines) Pv. The data for $MgSiO_3$ were obtained from Chopelas (1996).

except for v_3 for which $\Delta v = 13$ cm^{-1}) than the mode related to a breathing vibration of the GeO_6 octahedra, v_6, which shows $\Delta v = 20$ cm^{-1}. The low sensitivity of this mode to cation substitution is consistent with the mode assignment because a breathing vibration of the GeO_6 octahedra is not involved with motion of Ge atoms as they are at centrosymmetric positions. Yet, the slightly high frequency in $MgSiO_3$–Pv would be explained by higher bond strength of Si–O than Ge–O. However, it is interesting that the difference decreases with P (Fig 6).

Another similarity between $MgGeO_3$– and $MgSiO_3$–Pv is that P-induced mode shift is highly nonlinear. Chopelas (1996) attributed to a structural change at 40 GPa and fitted the trends separately below and above 40 GPa (Fig. 6). However, no X-ray diffraction study has identified a structural change in $MgSiO_3$–Pv near 40 GPa (Fiquet et al., 1998; Shim et al., 2001). Although we do not resolve any clear evidence of sharp changes in slopes in $MgGeO_3$, the modes shift with higher rates at lower P, which can be due to the metastability of the Pv phase.

Because frequencies and intensities of the modes are very similar between $MgSiO_3$– and $MgGeO_3$–Pv and the axial ratios between $MgSiO_3$– and $MgGeO_3$–PPv are in agreement within 2% (Kubo et al., 2006), it is expected that the mode intensities and frequencies would be similar between $MgGeO_3$– and $MgSiO_3$–PPv. Raman spectra of $MgSiO_3$–PPv have been calculated using the density functional perturbation theory (Caracas and Cohen, 2006). Mode frequencies between theory for $MgSiO_3$–PPv and our measurement for $MgGeO_3$–PPv are significantly different. From our comparison between $MgGeO_3$– and $MgSiO_3$–Pv as well as previous studies on ilmenite and pyroxene phases in $MgSiO_3$ and $MgGeO_3$ (McMillan and Ross, 1987; Ross and Navrotsky, 1988), it is expected that mode frequencies should be systematically higher by 20–80 cm^{-1} in $MgSiO_3$. However, no such correlation can be found between our measurements on $MgGeO_3$–PPv and calculated Raman frequencies for $MgSiO_3$–PPv (Fig. 5). Furthermore, the highest frequency mode in $MgGeO_3$–PPv is greater than that calculated for $MgSiO_3$–PPv.

Raman mode frequencies predicted by first-principles methods have shown reasonable agreements with observations. Predicted mode frequencies of $MgSiO_3$–Pv agree within $\Delta v = \pm 19$ cm^{-1} (Karki et al., 2000; Caracas and Cohen, 2006). For $MgAl_2O_4$ spinel, the difference is smaller than $\Delta v = \pm 8$ cm^{-1} (Lazzeri and Thilbaudeau, 2006). A recent calculation on Mg_2SiO_4 forsterite predicted systematically higher frequencies but the difference did not exceed 20 cm^{-1} (Noel et al., 2006). Therefore, the discrepancies between our measurements and first-principles appear significant.

It is notable that $MgGeO_3$–PPv has very high frequency modes, e.g., 1063 cm^{-1}, whereas the highest mode frequency in $MgGeO_3$–Pv is 718 cm^{-1} at 65 GPa. The GeO_6 (SiO_6) octahedra are connected by both edges and corners in PPv, whereas they are linked by the corners only in Pv (Murakami et al., 2004; Oganov and Ono, 2004). We found that the extrapolated frequencies of N_9 (802 cm^{-1}) and N_{10} (861 cm^{-1}) to 0 GPa are indeed similar to the frequency of the B_{2g} modes in rutile-structured GeO_2 (870 cm^{-1}) (Scott, 1970) and SiO_2 (967 cm^{-1}) (Hemley et al., 1986) which have the octahedra connected by both edges and corners. An intense high-frequency Raman mode has been documented in the ilmenite phases in $MgGeO_3$ at 722 cm^{-1} (Ross and Navrotsky, 1988) and in $MgSiO_3$ at 798 cm^{-1} (Reynard et al., 1996). The octahedra in ilmenite phases are connected by edges. These highest-frequency modes are related to stretching motion of Ge–O (Si–O) bonds in the octahedra (Hofmeister and Ito, 1992). Therefore, we postulate that the existence of the higher-frequency modes in PPv is connected to the Ge–O stretching vibrations in the octahedra with edge sharing.

4.2. Thermodynamic implications

Measurements of P-induced shifts of phonon modes allow us to calculate mode Grüneisen parameters,

$$\gamma_i = \frac{\partial \ln \omega_i}{\partial \ln V}, \tag{1}$$

where ω_i is the frequency of mode i. Together with Eq. (1), we use the following relation in order to constrain γ_i from our Raman data:

$$\gamma_i = \gamma_{i,r}\left(\frac{V}{V_r}\right)^q, \tag{2}$$

where q is the logarithmic volume derivative of the Grüneisen parameter, which is assumed to be a constant, and subscript r denotes the reference conditions. The volume at different pressures can be obtained from the EOS of $MgGeO_3$–Pv and –PPv (Kubo et al., 2006; Runge et al., 2006). We set the reference conditions to 65 GPa where the PPv transition is reported in $MgGeO_3$ (Hirose et al., 2005), because (1) we are interested in changes across the PPv transition and (2) Pv and PPv phases show some evidence of transitions during decompression near ambient conditions. Therefore, we limit ourselves to using the data points between 14 and 51 GPa (compression and

decompression) and between 83 and 123 GPa (compression only) for Pv and PPv, respectively.

In most previous studies of this type, frequency has been fitted to a polynomial function of pressure and then the derivative has been used to obtain γ_i. However, this *ad hoc* method can result in an increase of γ_i with P when frequencies are fitted to a linear function of P (Hofmeister and Mao, 2002). Such an increase is unphysical for a crystalline phase within its stability field, except for modes related to instability of the structure. Our approach of combining Eqs. (1) and (2) avoids this problem and requires γ_i to be volume independent if no clear nonlinearity can be resolved from the data. In this case, the resulting γ_i can be viewed as an average over the P range where data were measured. In fact, our scheme provides statistically as good results as a simple polynomial fitting scheme. For $MgGeO_3$–Pv, we found 4 modes with statistically significant volume dependences of γ_i (Table 1). However, we were not able to resolve the volume dependence of γ_i for PPv.

By using the following weighting scheme, we can obtain the average Grüneisen parameter:

$$\overline{\gamma} = \frac{\sum_i C_i \gamma_i}{\sum_i C_i} \tag{3}$$

where C_i is the Einstein heat capacity. We obtained 1.56±0.10 and 1.15±0.06 for Pv and PPv at 65 GPa, respectively. Simple averages give 1.55 and 1.17 for the two phases. Thus, the Grüneisen parameter decreases by 25±6% across the PPv transition in $MgGeO_3$. However, a first-principles study predicted that change in the Grüneisen parameter would be very small, only 2% decrease in magnitude (Tsuchiya et al., 2005).

In our approach the effect from dispersion is not included, and only 12% and 33% of expected normal modes are used for Pv and PPv, respectively. Nevertheless, it has been shown that $\overline{\gamma}$ agrees well with thermodynamic Grünisen parameter, γ_{th}, for many mantle minerals. For example, although only 19 Raman modes out of 84 total modes were used for forsterite, $\overline{\gamma}$ (1.09) agrees well with γ_{th} (1.17) (Chopelas, 1990). Good agreement was also found for Mg_2SiO_4-spinel, $\overline{\gamma}$=1.10 and γ_{th}=1.25 (Chopelas et al., 1994), although only 5 Raman modes out of 42 total modes were used. Hofmeister and Mao (2002) attributed this agreement to the fact that Raman-active modes are involved in vibrations at the whole unit-cell level.

Assuming the spectroscopic γ gives a reasonable approximation to γ_{th}, from the definition of γ_{th}, we can derive the following relations,

$$\frac{\alpha_{PPv}}{\alpha_{Pv}} = \frac{\gamma C_V / V K_T|_{PPv}}{\gamma C_V / V K_T|_{Pv}} \tag{4}$$

where C_V is the heat capacity and K_T is the isothermal bulk modulus. At high temperature (Dulong–Petit limit), C_V becomes $3R$ (R is the gas constant). From the EOS of $MgGeO_3$–Pv and PPv, V and K_T can be calculated. Thermal effect is included using the Grüneisen parameters we obtained and the Mië–Grüneisen equation. We found that this yields about

Table 1
Frequencies, mode Grüneisen parameters (γ_i), and q (=d ln γ/$d$ln$V$) of the Raman modes of $MgGeO_3$–Pv and PPv at 65 GPa and 300 K

Perovskite				Post-perovskite		
Frequency (cm^{-1})		γ_i	q_i	Frequency (cm^{-1})		γ_i [a]
0 GPa [b]	65 GPa			0 GPa [b]	65 GPa	
195±3	305±2	1.99±0.13	1.29±0.81	187±4	217±1	0.76±0.07
221±1	335±2	2.10±0.13	[a]	220±3	277±1	1.14±0.05
269±1	346±1	1.27±0.08	[a]	346±3	446±1	1.26±0.03
355±3	461±2	1.18±0.08	1.18±0.85	366±3	468±1	1.22±0.04
352±3	491±1	1.04±0.06	4.58±0.67	537±3	705±1	1.35±0.02
481±3	694±1	1.39±0.05	2.82±0.43	553±3	719±1	1.30±0.02
497±1	718±1	1.87±0.03	[a]	556±3	726±2	1.33±0.10
				711±3	881±1	1.06±0.12
				802±3	1030±1	1.24±0.01
				861±3	1063±1	1.05±0.01

Fitting was performed for a standard state at 65 GPa. The frequencies at 0 GPa are obtained by extrapolating the fitting results. The lower frequency of v_5 than v_4 is due to the extrapolation. In fact, they are indistinguishable within the uncertainty.

[a] No significant volume dependence of γ_i is detected.

[b] Extrapolated to 0 GPa.

25±10% decrease in thermal expansion parameter across the PPv transition in $MgGeO_3$ at 65 GPa and 2000 K.

Assuming the same magnitude of changes across the PPv transition for $MgSiO_3$, we calculate the profiles of the thermal expansion and Grüneisen parameter of mantle minerals as a function of pressure (or depth) along 2000 K isotherm (Fig. 7). We use the Mië–Grüneisen–Birch–Murnaghan equation of state (Jackson and Rigden, 1996; Shim and Duffy, 2000). Thermoelastic parameters of mantle silicates are obtained from Ita and Stixrude (1992) and Jackson and Rigden (1996) (and references therein). The Grüneisen parameter increases across most phase transitions in the mantle except for the wadsleyite-to-ringwoodite transition. The coordination number increase in some of the mantle transitions has been related to an increase in Grüneisen parameter (Stixrude and Karki, 2005). However, there is no coordination number change for Si across the PPv transition.

As shown above, thermal expansion parameter may decrease across the PPv transition. A similar magnitude of changes in thermal expansion parameter has been found for some other mantle transitions (Fig. 7). These changes across the PPv transition may have important implications for the bottommost mantle. For example, a discontinuous decrease in thermal expansivity across the PPv transition may dynamically stabilize the PPv layer.

The Clapeyron slope of the PPv transition can be obtained through the following relation:

$$\frac{dP}{dT} = \frac{\Delta S_{tr}}{\Delta V_{tr}}, \tag{5}$$

where ΔS_{tr} and ΔV_{tr} are the changes in entropy and volume across the phase transition. Following the method of Kieffer (1979a), entropy can be estimated from vibrational spectroscopy together with an assumed shape of phonon density of states (PDOS). Among the required parameters for the calculation, longitudinal and transverse wave velocities have not been measured for $MgGeO_3$–Pv and –PPv. We first calculate the bulk sound speed from the EOS (Kubo et al., 2006; Runge et al., 2006). Then the ratio between P and S wave velocities is estimated from the first-principles calculations for $MgSiO_3$–Pv and PPv (Wentzcovitch et al., 2006). Two averaged shear wave velocities are calculated using the estimated shear wave splitting of 7–10% from first-principles calculations (Wentzcovitch et al., 2006).

For the entropy contribution from the optic modes, we use PDOS consisting of single continua for Pv and PPv. The lower and upper limits of the continua are

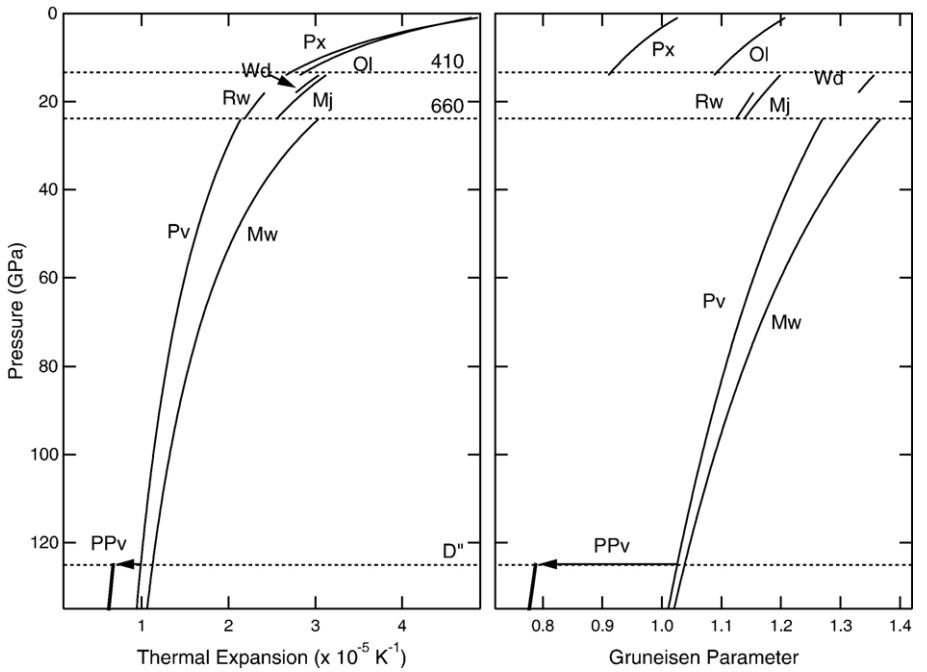

Fig. 7. Thermal expansion and Grünisen parameters of mantle silicates and oxides at high P and 2000 K. The dotted horizontal lines indicate the conditions corresponding to the 410, 660, and D'' discontinuities (Ol: olivine, Wd: wadsleyite, Rw: ringwoodite, Px: pyroxene, Mj: majorite, Pv: perovskite, Mw: magnesiowüstite, PPv: post-perovskite). Uncertainties in these parameters are 5–10%.

calculated from our Raman measurements using the scheme suggested by Kieffer (1979a). The volume change across the PPv transition is obtained from the EOS of $MgGeO_3$–Pv and –PPv (Kubo et al., 2006; Runge et al., 2006). We also take into account thermal effects on volume and mode frequencies using the Grüneisen and thermal expansion parameters obtained above. ΔV_{tr} for the PPv transition is −0.65 cm^3/mol at 2000 K and 65 GPa. From this model we obtain ΔS_{tr}=−12.9 $J \cdot mol^{-1} \cdot K^{-1}$, resulting in dP/dT=+20 MPa/K. The strong positive Clapeyron slope is consistent with the predictions for $MgSiO_3$, +7∼+10 MPa/K (Oganov and Ono, 2004; Tsuchiya et al., 2004; Sternik and Parlinski, 2006).

It is important to point out that the shapes of the PDOS functions are assumed and only Raman-active phonon modes at the Brillouin zone center are used in our calculation. Nevertheless, Clapeyron slopes estimated using this approach have shown good agreement with phase equilibria studies and calorimetry measurements in magnesium silicates (Akaogi et al., 1984; Lu and Hofmeister, 1994) and germanates (Ross and Navrotsky, 1987, 1988). Furthermore, the Clapeyron slopes of the phase transitions in $MgGeO_3$ and their counterparts in $MgSiO_3$ show similar magnitudes with same signs: +2.6±1.3 MPa/K in germanate (Ross and Navrotsky, 1988) and +3.1 (Pacalo and Gasparik, 1990) ∼+4.5 MPa/K (Ulmer and Stalder, 2001) in silicate for a transition from orthoenstatite to high-P clinoenstatite, −8.2 MPa/K in germanate (Akaogi et al., 2005) and −2.9 ∼−3.5 MPa/K in silicate (Ono et al., 2001) for a transition from ilmenite to perovskite.

The assumptions we used for the acoustic modes could result in some uncertainty in the entropy calculation. We found that a ±15% variation (within a reasonable range of Poisson's ratio) in the assumed ratio between P and S wave velocities results in variation of Clapeyron slope less than ±5 MPa/K. Varying the amount of shear wave splitting up to 50% does not change the slope more than ±2 MPa/K. This relatively low sensitivity (5–10%) is because the contribution from the acoustic modes is much smaller than that from the optic modes.

An important limitation of our estimation is that we measure only 7 of 24 Raman modes of Pv. In the studies by Chopelas (1996) and Williams et al. (1987), a mode at 499 cm^{-1} was the highest-frequency Raman mode in $MgSiO_3$–Pv, which seems to be related to v_6 of $MgGeO_3$–Pv (481 cm^{-1} at 0 GPa). A mode at 542 cm^{-1} has been observed in some ambient pressure Raman measurements (Wang et al., 1994; Liu et al., 1994; Gillet et al., 2000), which could be related to v_7 of $MgGeO_3$–Pv (497 cm^{-1} at 0 GPa). However, Gillet et al. (2000) and Durben and Wolf (1992) documented a mode at even higher frequency, i.e., 666 cm^{-1}, at ambient conditions in $MgSiO_3$–Pv. This mode is extremely weak and has never been observed at high P. Furthermore, we found that the high-frequency region (above 600 cm^{-1}) starts to gain some intensity during decompression outside the stability field of Pv. Therefore, caution must be exercised for features that are only observed at low P because of the potential instability of metastable Pv under intense laser radiation.

In order to examine the effect of possible missing DOS at higher frequency, we calculate entropy assuming an upper limit at 800 cm^{-1} for Pv at 65 GPa, whereas we use the same optic continuum for PPv. This yields a Clapeyron slope of +4 GPa/K. However, there could be undetected DOS at lower frequency for Pv which would then increase the Clapeyron slope. Considering all these factors, we believe a reasonable estimate for uncertainty (1σ) for the Clapeyron slope is ± 10 MPa/K.

The PDOS has been estimated for $MgSiO_3$–Pv and PPv by first-principles calculations (Karki et al., 2000; Tsuchiya et al., 2005; Sternik and Parlinski, 2006). These calculations show reasonable agreement in that both Pv and PPv show a block of DOS at low to mid-frequency range and an isolated peakshaped structure

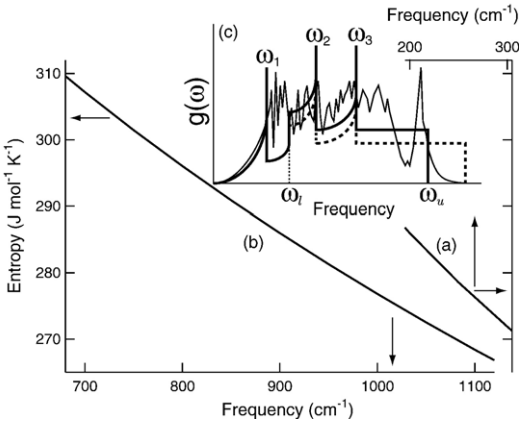

Fig. 8. Variations in estimated entropy from an optic continuum for PPv by changing (a) lower limit for a fixed upper limit (900 cm^{-1}) and (b) upper limit for a fixed lower limit (200 cm^{-1}). Frequency increases in the high-frequency modes across the PPv transition result in a decrease in the entropy of PPv. Although frequency decrease in the low-frequency modes may increase the entropy of PPv, the magnitude of the change is smaller for the observed changes in low-frequency region. (c) A hypothetical PDOS (thin curve) together with different Kieffer-type models with different upper limits (ω_{1-3}: maximum frequency of each acoustic branch, ω_l and ω_u: lower and upper limits of a Kieffer-type optic continuum).

near upper frequency limits, similar to a hypothetical DOS shown in Fig. 8c. The optic contribution to the DOS of PPv by Tsuchiya et al. (2005) exists between 150 and 910 cm^{-1}, which is in good agreement with the range bounded by our Raman measurements of $MgGeO_3$, i.e., 187–861 cm^{-1} at 0 GPa. At the PPv transition pressure, the predicted PDOS by theory for Pv and PPv are extended to a similar frequency, e.g., 1120–1130 cm^{-1} (Sternik and Parlinski, 2006), unlike our measurements. The discrepancy in the frequency range for Pv is too large to be explained by difference in the octahedrally coordinated cations (Si vs. Ge) and may indicate that some high-frequency Pv modes may not be detected in our Raman measurement.

Nevertheless, the predicted PDOS by theory shows some features that are consistent with our spectroscopically estimated PDOS in that more DOS exists at higher frequency region in PPv than Pv. The intensity of the high-frequency isolated peak in the DOS is higher in PPv by 40% (Sternik and Parlinski, 2006). More clear comparison can be made for the PDOS of $NaMgF_3$ estimated by Umemoto et al. (2006) at the PPv transition (Fig. 3a of their paper). An isolated high-frequency peak-shaped structure centered at 640 cm^{-1} in Pv shifts to 690 cm^{-1} in PPv.

In order to investigate the source of the entropy decrease across the PPv transition, we calculate entropies from optic continua with different limits (Fig. 8). When the lower limit decreases by 100 cm^{-1}, which is similar to the lower limit change from Pv to PPv in our Raman measurements, entropy increases by 15 $J{\cdot}mol^{-1}{\cdot}K^{-1}$. When the upper limit increases by 400 cm^{-1}, similar to the change from Pv to PPv, for a fixed lower limit, the entropy decreases as much as 40 $J{\cdot}mol^{-1}{\cdot}K^{-1}$. Due to the potential existence of missing high-frequency Pv modes as discussed above, our estimation for ΔS_{tr} should be regarded as an upper bound. Nevertheless, both the features observed in the PDOS predicted by first-principles calculations and the frequency range difference detected by our Raman study support an increase in PDOS at high-frequency region in PPv. Our model calculation shows that the lower entropy of PPv may result from this PDOS increase at high frequency in PPv.

High-frequency modes are related to the Ge–O (Si–O) stretching motion in the GeO_6 (SiO_6) octahedra (Hemley et al., 1986; Haines et al., 1998). The increase in DOS of PPv at higher frequency can be rationalized by the fact that there are edge-shared as well as corner-shared octahedra whereas all octahedra in Pv are linked by the corners. Therefore, the Ge–O (Si–O) bond strength would be higher in PPv than Pv. In fact, as pointed out by Lu and Hofmeister (1994), the highest-frequency mode of $MgSiO_3$–Pv is lower than their counterparts in ilmenite and stishovite which have the edge shared SiO_6 octahedra, whereas, as we discussed above, the highest-frequency mode of $MgGeO_3$–PPv is comparable to those of ilmenite-and rutile-type phases in germanates and silicates.

Another expected consequence from change in the linkage of the GeO_6 octahedra is that vibrations of some oxygen atoms would be more restricted in PPv due to the edge sharing, unlike Pv where the vibration of oxygen atoms are less restricted due to the corner sharing. Therefore, vibrations involved with bending of the Ge–O–Ge bonds and deformation of the Mg–O polyhedra would have higher frequency in PPv than Pv. This will lead to positive shifts of DOS at low frequency, leading to an entropy decrease after the PPv transition, as the bending and deformational modes exist in lower-frequency region. Unfortunately this cannot be confirmed by our data, as vibrational spectroscopy at the zone center cannot constrain the DOS directly. However, this can be seen in the comparison of DOS of Pv and PPv in $NaMgF_3$ presented by Umemoto et al. (2006): DOS below 170 cm^{-1} is higher in Pv than PPv, although existence of acoustic modes in this range make clear comparison difficult.

5. Conclusion

Our Raman measurements show that PPv has intense modes at high frequency, i.e., 880–1063 cm^{-1} at 65 GPa, whereas the highest-frequency mode in Pv exists at 718 cm^{-1}. The appearance of the high-frequency modes in PPv is related to the formation of the edge sharing between the GeO_6 octahedra across the PPv transition which would make the Ge–O bonds stronger.

Measured *P*-induced shifts of the Raman modes suggest significant decreases in the Grüneisen parameter and the thermal expansivity across the PPv transition. If a similar change occurs in $MgSiO_3$, the discrete decrease in the thermal expansion parameter across the PPv transition would dynamically stabilize the PPv layer at the lowermost mantle. Our estimated Clapeyron slope of the PPv transition is $+20\pm10$ MPa/K. The strong positive slope is consistent with the predictions for the PPv transition in $MgSiO_3$, +7∼+10 MPa/K (Oganov and Ono, 2004; Iitaka et al., 2004; Tsuchiya et al., 2004; Sternik and Parlinski, 2006).

Our model calculations suggest that the lower entropy of PPv may result at least partly from an increase in phonon density of states (PDOS) at high

frequency across the transition due to the formation of the edge shared GeO_6 octahedra. Vibration of oxygen atoms and deformation of the MgO_8 polyhedra would be more restricted in PPv, resulting in a positive shift of PDOS at lower frequency and consequently a decrease in entropy. These interpretations are in qualitative agreement with recent estimation of PDOS by first-principles calculations.

We note that our Raman measurements provide partial information on the PDOS of Pv and PPv. Infrared spectroscopy measurements on Pv and PPv at in situ high P will enhance the accuracy of the modeling results. In particular, detecting more phonon modes of Pv at high pressure is critical to better constrain the Clapeyron slope. The discrepancy on the Raman spectra of PPv between our measurements and theoretical calculations should be carefully examined. Nevertheless, our results support the strong positive Clapeyron slope of the PPv transition and reveal that change in the connectivity among the octahedra may have profound impact on the slope. Finally, vibrational spectroscopy measurements on $MgSiO_3$–PPv will provide more direct constraints on the thermodynamic property changes across the PPv transition, although several technical issues need to be addressed carefully.

Acknowledgments

This work is supported by NSF (EAR-0337005) to DS. Construction of the Raman and laser heating systems at MIT were possible from the support by NSF (EAR-0337156) and the Wade fund to DS. We thank R. J. Cava (Chemistry Dept. Princeton) for use of his sample synthesis facility. We thank an anonymous reviewer and R. Jeanloz for helpful discussions.

References

Akaogi, M., Ross, N.L., McMillan, P., Navrotsky, A., 1984. The Mg_2SiO_4 polymorphs (olivine, modified spinel, and spinel) — thermodynamic properties from oxide melt solution calorimetry, phase relations, and models of lattice vibrations. Am. Mineral. 69, 499–512.

Akaogi, M., Kojitani, H., Yusa, H., Yamamoto, R., Kido, M., Koyama, K., 2005. High-pressure transitions and thermochemistry of $MGeO_3$ (M = Mg, Zn, andSr) and Sr-silicates: systematics in enthalpies of formation of $A^{2+}B^{4+}O_3$ perovskites. Phys. Chem. Miner. 32, 603–613.

Boehler, R., 2000. High-pressure experiments and the phase diagram of lower mantle and core materials. Rev. Geophys. 38, 221–245.

Caracas, R., Cohen, R.E., 2006. Theoretical determination of the Raman spectraof $MgSiO_3$ perovskite and post-perovskite at high pressure. Geophys. Res. Lett. 33, L12S05.

Chopelas, A., 1990. Thermal properties of forsterite at mantle pressures derived from vibrational spectroscopy. Phys. Chem. Miner. 17, 149–156.

Chopelas, A., 1996. Thermal expansivity of lower mantle phases MgO and $MgSiO_3$ perovskite at high pressure derived from vibrational spectroscopy. Phys. Earth Planet. Inter. 98, 3–15.

Chopelas, A., 1999. Estimates of mantle relevant Clapeyron slopes in the $MgSiO_3$ system from high-pressure spectroscopic data. Am. Mineral. 84, 233–244.

Chopelas, A., Boehler, R., Ko, T., 1994. Thermodynamics and behavior of γ-Mg_2SiO_4 at high pressure: implications for Mg_2SiO_4 phase equilibrium. Phys. Chem. Miner. 21, 351–359.

Durben, D.J., Wolf, G.H., 1992. High-temperature behavior of metastable $MgSiO_3$ perovskite: a Raman spectroscopic study. Am. Mineral. 77, 890–893.

Eggert, J.H., Goettel, K.A., Silvera, I.F., 1988. Elimination of pressure-induced fluorescence in diamond anvils. Appl. Phys. Lett. 53, 2489–2491.

Fiquet, G., Andrault, D., Dewaele, A., Charpin, T., Kunz, M., Haüsermann, D., 1998. P–V–T equation of state of $MgSiO_3$ perovskite. Phys. Earth Planet. Inter. 105, 21–31.

Gillet, P., Daniel, I., Guyot, F., Matas, J., Chervin, J.-C., 2000. A thermodynamic model for $MgSiO_3$-perovskite derived from pressure, temperature and volume dependence of the Raman mode frequencies. Phys. Earth Planet. Inter. 117, 361–384.

Guignot, N., Andrault, D., Morard, G., Bolfan-Casanova, N., Mezouar, M., 2007. Thermoelastic properties of post-perovskite phase $MgSiO_3$ determined experimentally at core–mantle boundary P–T conditions. Earth Planet. Sci. Lett. 256, 162–168.

Haines, J., Léger, J.M., Chateau, C., Bini, R., Ulivi, L., 1998. Ferroelastic phase transition in rutile-type germanium dioxide at high pressure. Phys. Rev., B 58, R2909–R2912.

Hemley, R.J., Mao, H.-K., Chao, E.C.T., 1986. Raman spectrum of natural and synthetic stishovite. Phys. Chem. Miner. 13, 285–290.

Hernlund, J.W., Thomas, C., Tackley, P.J., 2005. A doubling of the post-perovskite phase boundary and structure of the Earth's lower most mantle. Nature 434, 882–886.

Hirose, K., Fujita, Y., 2005. Clapeyron slope of the post-perovskite phase transition in $CaIrO_3$. Geophys. Res. Lett. 32, L13313.

Hirose, K., Kawamura, K., Ohishi, Y., Tateno, S., Sata, N., 2005. Stability and equation of state of $MgGeO_3$ post-perovskite phase. Am. Mineral. 90, 262–265.

Hirose, K., Sinmyo, R., Sata, N., Ohishi, Y., 2006. Determination of post-perovskite phase transition boundary in $MgSiO_3$ using Au and MgO pressure standards. Geophys. Res. Lett. 33, L01310.

Hofmeister, A.M., Ito, E., 1992. Thermodynamic properties of $MgSiO_3$ ilmenite from vibrational spectra. Phys. Chem. Miner. 18, 423–432.

Hofmeister, A.M., Mao, H.-K., 2002. Redefinition of the mode Grüneisen parameter for polyatomic substances and thermodynamic implications. Proc. Natl. Acad. Sci. 99, 559–564.

Iitaka, T., Hirose, K., Kawamura, K., Murakami, M., 2004. The elasticity of the $MgSiO_3$ post-perovskite phase in the earth's lowermost mantle. Nature 430, 442–445.

Ita, J., Stixrude, L., 1992. Petrology, elasticity and composition of the mantle transition zone. J. Geophys. Res. 97, 6842–6866.

Jackson, I., Rigden, S.M., 1996. Analysis of P–V–T data: constraints on the thermoelastic properties of high-pressure minerals. Phys. Earth Planet. Inter. 96, 85–112.

Karki, B.B., Wentzcovitch, R.M., de Gironcoli, S., Baroni, S., 2000. Ab initio lattice dynamics of $MgSiO_3$ perovskite at high pressure. Phys. Rev., B 62, 14750–14756.

Kieffer, S.W., 1979a. Thermodynamics and lattice vibrations of minerals: 1. Mineral heat capacities and their relationships to simple lattice vibrational models. Rev. Geophys. Space Phys. 17, 1–19.

Kieffer, S.W., 1979b. Thermodynamics and lattice vibrations of minerals: 3. Lattice dynamics and an approximation for minerals with application to simple substances and framework silicates. Rev. Geophys. Space Phys. 17, 35–59.

Kieffer, S.W., 1982. Thermodynamics and lattice vibrations of minerals: 5. Applications to phase equilibria, isotopic fractionation, and high-pressure thermodynamic properties. Rev. Geophys. Space Phys. 20, 827–849.

Kiefer, B., Duffy, T.S., 2005. Finite element simulations of the laser-heated diamond-anvil cell. J. Appl. Phys. 97, 114902.

Kubo, A., Kiefer, B., Shen, G., Prakapenka, V.B., Cava, R.J., Duffy, T.S., 2006. Stability and equation of state of the post-perovskite phase in $MgGeO_3$ to 2 Mbar. Geophys. Res. Lett. 33, L12S12.

Lay, T., Heinz, D., Ishii, M., Shim, S.-H., Tsuchiya, J., Tsuchiya, T., Wentzcovitch, R., Yuen, D., 2005. Multidisciplinary impact of the deep mantle phase transition in perovskite structure. EOS Trans. 86 (1), 1–4.

Lay, T., Hernlund, J., Garnero, E.J., Thorne, M.S., 2006. A post-perovskite lens and D'' heat flux beneath the central pacific. Science 314, 1272–1276.

Lazzeri, M., Thilbaudeau, P., 2006. Ab initio Raman spectrum of the normal and disordered $MgAl_2O_4$ spinel. Phys. Rev., B 74, 140301.

Liu, L.-G., Mernagh, T.P., Irifune, T., 1994. High pressure Raman spectra of β-Mg_2SiO_4, γ-Mg_2SiO_4, $MgSiO_3$-ilmenite, and $MgSiO_3$-perovskite. J. Phys. Chem. Solids 55, 185–193.

Lu, R., Hofmeister, A.M., 1994. Thermodynamic properties of ferromagnesium silicate perovskites from vibrational spectroscopy. J. Geophys. Res. 99, 11795–11804.

Mao, H.-K., Xu, J., Bell, P.M., 1986. Calibration of the ruby pressure gauge to 800 kbar under quasihydrostatic conditions. J. Geophys. Res. 91, 4673–4676.

Matyska, C., Yuen, D.A., 2005. The importance of radiative heat transfer on superplumes in the lower mantle with the new post-perovskite phase change. Earth Planet. Sci. Lett. 234, 71–81.

McMillan, P.F., Ross, N.L., 1987. Heat capacity calculations for Al_2O_3 corundum and $MgSiO_3$ ilmenite. Phys. Chem. Miner. 14, 225–234.

Merkel, S., Kubo, A., Miyagi, L., Speziale, S., Duffy, S., Mao, H.-K., Wenk, H.-R., 2006. Plastic deformation of $MgGeO_3$ post-perovskite at lower mantle pressures. Science 311, 644–646.

Miyajima, N., Ohgushi, K., Ichihara, M., Yagi, T., 2006. Crystal morphology anddislocation microstructures of $CaIrO_3$: A TEM study of an analogue of the $MgSiO_3$ post-perovskite phase. Geophys. Res. Lett. 33, L12302.

Murakami, M., Hirose, K., Kawamura, K., Sata, N., Ohishi, Y., 2004. Postperovskite phase transition in $MgSiO_3$. Science 304, 855–858.

Nakagawa, T., Tackley, P.J., 2004. Effects of a perovskite–post perovskite phase change near core–mantle boundary in compressible mantle convection. Geophys. Res. Lett. 31, L16611.

Noel, Y., Catti, M., D'Arco, Ph., Dovesi, R., 2006. The vibrational frequencies of forsterite Mg_2SiO_4: an all-electron ab initio study with the CRYSTAL code. Phys. Chem. Miner. 33, 383–393.

Oganov, A.R., Ono, S., 2004. Theoretical and experimental evidence for a postperovskite phase of $MgSiO_3$ in Earth's D'' layer. Nature 430, 445–448.

Ono, S., Katsura, T., Ito, E., Kanzaki, M., Yoneda, A., Walter, M.J., Urakawa, S., Utsumi, W., Funakoshi, K., 2001. In situ observation of ilmenite-perovskitephase transition in $MgSiO_3$ using synchrotron radiation. Geophys. Res. Lett. 28, 835–838.

Pacalo, R.E.G., Gasparik, T., 1990. Reversals of the orthoenstatite–clinoenstatite transition at high pressures and temperatures. J. Geophys. Res. 95, 15853–15858.

Reynard, B., Takir, F., Guyot, F., Gwanmesia, G.D., Liebermann, R.C., Gillet, P., 1996. High-temperature Raman spectroscopic and X-ray diffraction study of β-Mg_2SiO_4: insights into its high-temperature thermodynamic propoerties and the β- to α-phase-transformation mechanism and kinetics. Am. Mineral. 81, 585–594.

Ross, N.A., Navrotsky, A., 1987. The Mg_2GeO_4 olivine-spinel phase transition. Phys. Chem. Miner. 14, 473–481.

Ross, N.L., Navrotsky, A., 1988. Study of the $MgGeO_3$ polymorphs (orthopyroxene, clinopyroxene, and ilmenite structures) by calorimetry, spectroscopy, and phase equilibria. Am. Mineral. 73, 1355–1365.

Runge, C.E., Kubo, A., Kiefer, B., Meng, Y., Prakapenka, V.B., Shen, G., Cava, R.J., Duffy, T.S, 2006. Equation of state of $MgGeO_3$ perovskite to 65 GPa: comparison with the post-perovskite phase. Phys. Chem. Miner. 33, 699–709.

Santillán, J., Shim, S.-H., Shen, G., Prakapenka, V.B., 2006. High-pressure phase transition in bixbyite — application for the crystal structure and properties of the $CaIrO_3$–type. Geophys. Res. Lett. 33, L15307.

Scott, J.F., 1970. Raman spectra of GeO_2. Phys. Rev., B 1, 3488–3493.

Shim, S.-H., 2005. Stability of $MgSiO_3$ perovskite in the lower mantle. In: van der Hilst, R.D., Bass, J., Matas, J., Trampert, J. (Eds.), Earth's Deep Mantle: Structure, Composition, and Evolution. Geophysical Monograph Series, vol. 160. American Geophysical Union, pp. 261–282.

Shim, S.-H., Duffy, T.S., 2000. Constraints on the P–V–T equation of state of $MgSiO_3$ perovskite. Am. Mineral. 85, 354–363.

Shim, S.-H., Duffy, T.S., Shen, G., 2001. Stability and structure of $MgSiO_3$ perovskite to 2300-km depth conditions. Science 293, 2437–2440.

Shim, S.-H., Duffy, T.S., Kenichi, T., 2002. Equation of state of gold and its application to the phase boundaries near the 660-km depth in the mantle. Earth Planet. Sci. Lett. 203, 729–739.

Shim, S.-H., Duffy, T.S., Jeanloz, R., Shen, G., 2004. Stability and crystal structure of $MgSiO_3$ perovskite to the core–mantle boundary. Geophys. Res. Lett. 31, L10603.

Sidorin, I., Gurnis, M., Helmberger, D.V., 1999. Evidence for a ubiquitous seismic discontinuity at the base of the mantle. Science 286, 1326–1331.

Sternik, M., Parlinski, P., 2006. Ab initio calculations of the stability and lattice dynamics of the $MgSiO_3$ post-perovskite. J. Phys. Chem. Solids 67, 796–800.

Stixrude, L., Karki, B., 2005. Structure and freezing of $MgSiO_3$ liquid in Earth's lower mantle. Science 310, 297–299.

Tsuchiya, T., Tsuchiya, J., Umemoto, K., Wentzcovitch, R.M., 2004. Phase transition in $MgSiO_3$ perovskite in the earth's lower mantle. Earth Planet. Sci. Lett. 224, 241–248.

Tsuchiya, J., Tsuchiya, T., Wentzcovitch, R.M., 2005. Vibrational and thermodynamic properties of $MgSiO_3$ postperovskite. J. Geophys. Res. 110, B02204.

Ulmer, P., Stalder, R., 2001. The $Mg(Fe)SiO_3$ orthoenstatite–clinoenstatite transitions at high pressures and temperatures determined by Raman-spectroscopy on quenched samples. Am. Mineral. 86, 1267–1274.

Umemoto, K., Wentzcovitch, R.M., Weidner, D.J., Parise, J.B., 2006. $NaMgF_3$: a low-pressure analog of $MgSiO_3$. Geophys. Res. Lett. 33, L15304.

van der Hilst, R.D., de Hoop, M.V., Wang, P., Shim, S.-H., Ma, P., Tenorio, L., 2007. Seismo-stratigraphy and thermal structure of Earth's core–mantle boundary region. Science 315, 1813–1817.

Wang, Y., Weidner, D.J., Liebermann, R.C., Zhao, Y., 1994. P–V–T equation of state of (Mg,Fe)SiO_3 perovskite: constraints on composition of the lower mantle. Phys. Earth Planet. Inter. 83, 13–40.

Wentzcovitch, R.M., Tsuchiya, T., Tsuchiya, J., 2006. $MgSiO_3$ postperovskite at D'' conditions. Proc. Natl. Acad. Sci. 103, 543–546.

Williams, Q., Jeanloz, R., McMillan, P., 1987. Vibrational-spectrum of $MgSiO_3$ perovskite — zero-pressure Raman and midinfrared spectra to 27 GPa. J. Geophys. Res. 92, 8116–8128.

Xu, J., Mao, H.-K., Bell, P.M., 1986. High pressure ruby and diamond fluorescence: observations at 0.21 to 0.55 terapascal. Science 232, 1404–1406.